Fang, Wenwen; Nonappa; Vitikainen, Marika; Mohammadi, Pezhman; Koskela, Salla; Soikkeli, Miika; Westerholm-Parvinen, Ann; Landowski, Christopher P.; Penttilä, Merja; Linder, Markus B.; Laaksonen, Päivi

Coacervation of resilin fusion proteins containing terminal functionalities

Published in:
Colloids and Surfaces B: Biointerfaces

DOI:
10.1016/j.colsurfb.2018.07.048

Published: 01/11/2018

Document Version
Peer-reviewed accepted author manuscript, also known as Final accepted manuscript or Post-print

Coacervation of resilin fusion proteins containing terminal functionalities

Wenwen Fang[a], Nonappa[a,b], Marika Vitikainen[c], Pezhman Mohammadi[a], Salla Koskela[c], Miika Soikkeli[c], Ann Westerholm-Parvinen[c], Christopher P. Landowski[c], Merja Penttilä[a,c], Markus B. Linder[a], Päivi Laaksonen[*a]

a. Department of Bioproducts and Biosystems, Aalto University, Espoo, FI-00076 AALTO, Finland.

b. Department of Applied Physics, Aalto University, Espoo, FI-00076 AALTO, Finland.

c. VTT Technical Research Centre of Finland Ltd., Espoo, FI-02044 VTT, Finland

* Department of Bioproducts and Biosystems, Aalto University, Espoo, FI-00076 AALTO, Finland

Tel. +358504602611. E-mail: paivi.laaksonen@aalto.fi

Abstract

Liquid-liquid phase transition known as coacervation of resilin-like-peptide fusion proteins containing different terminal domains were investigated. Two different modular proteins were designed and produced and their behavior were compared to a resilin-like-peptide without terminal domains. The size of the particle-like coacervates was modulated by the protein concentration, pH and temperature. The morphology and three-dimensional (3D) structural details of the coacervate particles were investigated by cryogenic transmission electron microscopy (cryo-TEM) and tomography (cryo-ET) reconstruction. Selective adhesion of the coacervates on cellulose and graphene surfaces was demonstrated.

Key words

Resilin, self-assembly, coacervation, selective adhesion, tomography

1. Introduction

Proteins can undergo liquid-liquid phase transition where highly concentrated liquid-like droplets form and separate from aqueous phase. Such transition is called coacervation and it strongly influences functions and activity of certain proteins.[1] For example, coacervation of tropoelastin is the first vital step in elastic fiber formation.[2][3] The coacervate particles then progressively grow into larger assemblies and finally mature into fibrous structures.[4][5] According to recent findings, coacervation is essential in fundamental biological processes, *e.g*. promoting assembly of spindles.[6] From the point view of material science, coacervation is also very important for the functionalities of natural materials, such as the gradient stiffness of squid beak, underwater coatings and adhensives.[7][8]

Tropoelastin, as a representative protein that undergoes single coacervation, has been studied intensively. Its primary structure is considered to be the basis for this process, especially the hydrophobic domains are thought to directly affect the self-assembly.[5] Resilin is an elastomeric protein found in specialized regions of the cuticle of most insects. The protein has similar primary structure with tropoelastin, and both of them are regarded as intrinsically disordered proteins.[9][10][11] Resilin-like-peptides have been reported to undergo temperature-triggered phase separation.[11][12] However, there is limited knowledge on how functional terminal domains fused to the resilin-like-peptide affect the coacervation process and whether these will make the resilin coacervates functional.

In this work, resilin fusion proteins consisting of the exon I Rec1-resilin from *Drosophila melanogaster* with different adhesive terminal domains were constructed to design functional coacervates. The effect of different terminal domains on the coacervation of the resilin-like proteins was investigated by analyzing the coacervate size and morphology at different conditions. The functionality was studied by testing the adhesion of coacervated proteins on different materials. The three different constructs studied were the resilin-like-peptide (RLP), RLP with cellulose binding modules at both terminal ends (CBM-RLP-CBM) and RLP with double CBM at the N-terminal and a hydrophobin HFBI at the C-terminal end (dCBM-RLP-HFBI) (Figure 1). The schematic in Figure 1d and the hydrophobicity index in Figure 1e illustrates the repetitive sequence

of RLP. The fungal family I CBMs employed here are the non-catalytic domains of the cellobiohydrolase enzyme, which binds to cellulose crystals through a set of aromatic residues and hydrogen bonding (Figure 1f).[13][14] The second type of adhesive domain HFBI, is an amphiphilic protein having a hydrophobic patch able to form supramolecular multimers in aqueous conditions through hydrophobic interactions (Figure 1g).[15] Understanding the formation and added functionality of the coacervates is crucial for being able to employ them in, for instance, hybrid composite materials.

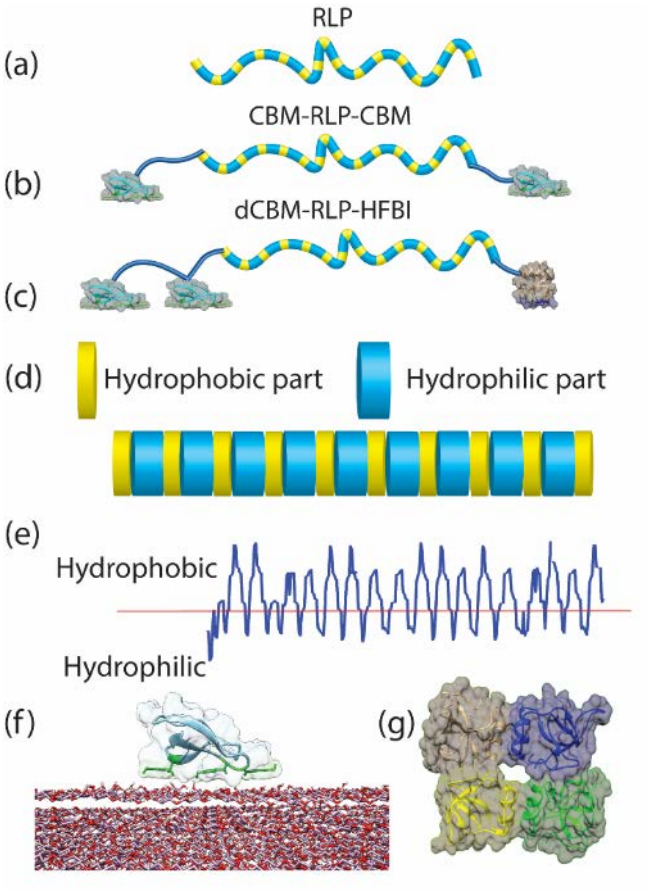

Figure 1. Schematics. Different protein constructs used in this work. (a) Resilin-like-peptide (RLP). (b) Cellulose binding module (CBM)-RLP-CBM. (c) dCBM-RLP-hydrophobin (HFBI). (d) Schematic structure of RLP. (e) Hydrophobicity index of RLP. (f) CBM binds to the surface of cellulose. (g) HFBI forms tetramers under aqueous environment due to the hydrophobic interactions.

2. Experimental

2.1 Protein production and purification

Synthetic Drosophila melanogaster Rec1-resilin fusion proteins were expressed in *Trichoderma reesei*. The production and purification of the proteins have been described earlier; RLP, CBM-RLP-CBM[16] and dCBM-RLP-HFBI[17].

2.2 Formation of the coacervates

The lyophilized resilin proteins were dissolved in water to obtain protein solutions with desired concentrations. 1M sodium phosphate buffers with different pHs were prepared and sterilized. The resilin coacervate was formed by mixing the resilin solutions with sodium phosphate buffer.

2.3 Cross linking of the coacervates

The horseradish peroxidase (lyophilized powder, Sigma Aldrich) was added to resilin solution first and then the phosphate buffer was added to trigger the coacervation. Finally, 40 mM hydrogen peroxide solution was added to accomplish the cross linking process.

2.4 Characterization by Attenuated Total reflection-Fourier Transform Infrared Spectroscopy (ATR-FTIR)

A Nicolet 380 FT-IR Spectrometer (Thermo Scientific) was used to characterize the conformational changes of resilin fusion protein coacervates. The CBM-RLP-CBM and dCBM-RLP-HFBI coacervates were formed with 500 mM sodium phosphate buffer at pH 7.14, and then separated by centrifugation at 10000 rpm. The separated/concentrated coacervates were then analyzed with ATR-FTIR. The CBM-RLP-CBM and dCBM-RLP-HFBI water solutions were used as reference.

2.5 Characterization by Scanning Electron Microscopy

The dCBM-RLP-HFBI coacervates were centrifuged at 10000 rpm to separate them from the free proteins. The separated coacervates were drop casted on silicon wafer and dried at room temperature. The cross linked dCBM-RLP-HFBI coacervates were washed by centrifugation at 10000 rpm and then drop-casted on silicon wafer. All the samples were sputtered with a thin layer of gold/platinum (Emitech K950X/K350) to prevent the charging of the samples. The coated samples were imaged using a field emission scanning electron microscope (Zeiss Sigma VP FE-SEM) under the acceleration voltages of 1−3 keV.

2.6 Characterization by Cryo-Transmission Electron Microscopy

The Cryo-TEM samples were prepared by placing 3.0 µL aqueous dispersion on a 200-mesh copper grid with either holey carbon support film (CF-Quantifoil) or lacey carbon support film and plunge freezed in 50/50 liquid propane/ethane mixture using vitrobot with 2s blotting time under 100% humidity. The transmission electron microscopy (TEM) images were collected using JEM 3200FSC field emission microscope (JEOL) operated at 300 kV in bright field mode with Omega-type Zero-loss energy filter. The images were acquired with GATAN DIGITAL MICROGRAPH software while the specimen temperature was maintained at -187°C.

2.7 Sample Preparation using sequential solvent exchange

The original sample (3.0 µL) was placed on a hexagonal 300 mesh TEM grid with ultrathin carbon film. Before adding the samples, the TEM grids were plasma cleaned for 30 seconds and treated with 5 nm fiducial gold markers. After placing the sample on a pretreated grid (1-2 min), the grids were washed with water followed by (50% MeOH/H2O v/v) and 3x MeOH for 15 sec. each. Further, the sequential washing was continued with 50% MeOH/tert-butanol and 3x tert-butanol and placed the grid in an Eppendorf containing 100 µL of tert-butanol. The excess tert-butanol was removed using micropipette before placing the samples in a lyophilizer for 1 hour. The dried specimen was used for imaging.

2.8 Serial Electron Microscopy and Electron Tomographic Reconstruction

Electron tomographic tilt series were acquired with the SerialEM-software package.[18] Samples were tilted between ±69º angles with 2-3º increment steps. Prealignment of tilt image series was and the fine alignment and cropping was executed with IMOD.[19] The images were binned twice to reduce noise and computation time. Maximum entropy method (MEM) reconstruction scheme was carried out with custom made program on Mac or Linux cluster with regularization parameter value of λ = 1.0e^{-3}.[20] The 3D isosurface and solid colored images were produced in Chimera after final reconstruction.

2.9 Dynamic Light Scattering

The particle size of CBM-RLP-CBM and RLP coacervates formed at different conditions was determined by photon correlation spectroscopy (PCS) on a Malvern Zetasizer 3000 (Malvern Instrument, Malvern, UK). All the samples were fresh prepared just before the measurements and stabilized for 120s before start the measurement. The measurements were performed three times for each sample.

2.10 Adsorption of coacervates on different surfaces

Graphene on Pt substrates

Graphene on Si substrates with 200 nm of sputtered Pt was grown by using a photo-thermal CVD process.[21] The substrates were pre-annealed at 800°C degrees for 5 min under hydrogen flow (15 sccm) at 1 Torr to crystalize the Pt. Then graphene was grown at 820°C degrees for 1 min under methane (12 sccm) and hydrogen (4 sccm) flow at 12 Torr.

Regenerated cellulose on SiO_2 substrates

The cellulose surface was prepared by convertion of trimethylsilyl cellulose (TMSC) to regenerated cellulose with HCl.[22] Before deposition, the silicon wafers were cleaned with piranha solution. The cleaned silicon wafers were then coated with 1 g L^{-1} of TMSC using a spin-coater. The regeneration of TMSC to cellulose was performed by vapour phase acid hydrolysis using 37 % HCl.

The adsorptions of RLP, CBM-RLP-CBM and dCBM-RLP-HFBI coacervates on graphene, cellulose and glass surfaces were measured by dipping the substrates into the coacervate suspension for 5 min, and then rinsed gently with deionized water. The coacervate coated substrates were dried at ambient conditions and then imaged with SEM. See the Electronic Supplementary Information.

3. Results and discussions

3.1 Coacervation of the resilin fusion proteins

Coacervation is a process where macromolecules phase separate and form a concentrated phase. Coacervation can be induced by various triggers such as increased ionic strength, temperature, concentration or the combination of these variables which will lead to the segregation of the component from the solvent and form a condensed phase.[3][12] In this study, the focus was on the ionic strength and pH induced coacervation of resilin-like-peptides. The experiments were carried out by dissolving RLPs in 500 mM sodium phosphate buffer at different pHs and the observing the phase separation behaviour. It is noteworthy to differentiate the single coacervation studied here, from the complex coacervation that is a result of electrostatic attraction between polyelectrolytes of opposite charges.

The conformational transitions during the salt-induced coacervation of the RLP fusion proteins were analyzed by attenuated total reflection-Fourier transform infrared spectroscopy (ATR-FTIR) (Figure S1). The absorbance band at 1670 cm^{-1} was assigned to the PPII conformation and was

obtained for the resilin fusion protein solutions.[23] After coacervation, the band at 1670 cm^{-1} shifted to 1634 cm^{-1}, which was assigned to the transition to the β-sheet conformation.[24] The FTIR study confirmed that there were conformational changes during the salt-induced coacervation.

The coacervation of the RLP fusion proteins were associated with conformational transitions, mainly the increased fraction of *β*-sheets, and the similar conformational transitions have also been found in tropoelastin and elastin-like polypeptides.[5][25] A previous study of the molecular and supramolecular structure of resilin has shown that transition from the PPII conformation to folded conformations leads to self-assembly and micro-structures.[23]

Coacervation of the different RLP constructs was affected by the ionic strength, pH, protein concentration and temperature. The sizes of the coacervate particles of RLP and CBM-RLP-CBM were measured by dynamic light scattering (DLS). The contribution of pH and protein concentration in the coacervate size for RLP and CBM-RLP-CBM is presented in Figure 2. The behaviour of the RLP and the CBM-RLP-CBM appears very similar, coacervation lead into spherical individual particles whose sizes varied from some hundreds of nanometers to several micrometers. The sharp increase of the particle size below 600 nm to the micrometer level was taken as the threshold for coacervation. In both cases, coacervation was triggered by increased concentration in a pH dependent way, where elevating the pH above 6 lead to formation of the micrometer-sized particles. The particle size increased further with increasing protein concentration.

The dCBM-RLP-HFBI formed spherical coacervate particles already at 2 g L^{-1} but the particles had high tendency towards clustering (Figure 2c and d). At higher protein concentrations, the strong scattering from the agglomerated particles complicated the DLS analysis and it was not possible to measure the precise size of the individual particles. In Figure 2c, typical DLS data of the 2 g L^{-1} samples showing a bimodal distribution based on the particle volume fraction is presented. Based on confocal microscopy (Figure 2d) and optical microscopy images (Figure S2), the peak

measured at 1.5 µm size range represents the individual coacervates and the larger peak near 6 µm the agglomerates. Overall, the dCBM-RLP-HFBI coacervates were more resistant to the environmental conditions and there was no clear differences of the coacervate size at different pH values.

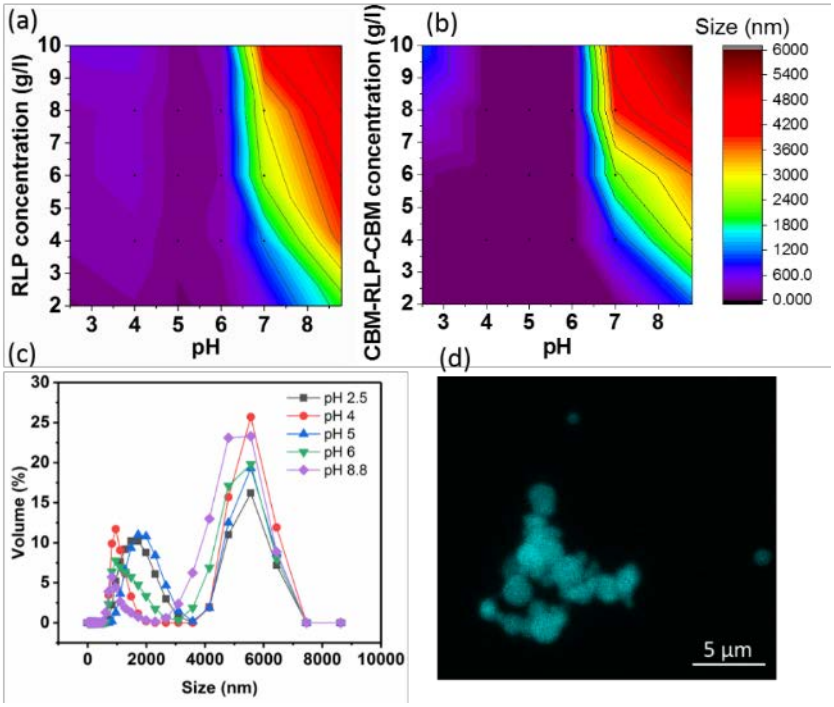

Figure 2. The effect of protein concentration and pH on the size of RLP coacervate (a) and CBM-RLP-CBM coacervate (b) in 500 mM phosphate buffer. The particle sizes were measured by dynamic light scattering (DLS). (c) The size distribution of 2 g L^{-1} dCBM-RLP-HFBI coacervate formed at different pH values. (d) Confocal microscopy image of dCBM-RLP-HFBI coacervate.

According to a previous study, the resilin molecule has compact conformation near the isoelectric point (IEP), but more extended one at pH significantly above and below the IEP.[16][17] Based on the Zeta-potential measured as a function of pH, the values of the IEP of the CBM-RLP-CBM and RLP were 4.5 and 4.9 accordingly.[16][26] For both RLP and CBM-RLP-CBM, the smallest coacervates were formed near the IEP, and larger coacervates were formed at higher pH above a certain concentration limit. In the Figure 2 b, a slightly increased size of the CBM-RLP-CBM

coacervates at low pH was observed at high protein concentration. The behaviour at high and low pHs indicates that the coacervation could be a consequence of the extended conformation of the individual proteins and the consequent increased interaction between the molecules that enables formation of large protein assemblies.[16][17] Based on the particle sizes, there was no obvious influence of the CBM domains on coacervation of RLP proteins.

3.2 Coacervate characteristics

The structure and morphology of the CBM-RLP-CBM coacervates at different pHs were imaged by cryo-TEM as shown in Figure 3. At pH 4.5 the CBM-RLP-CBM, formed very small coacervates, whose average diameter was near 50 nm (Figure 3a). At higher pH (7.14), the CBM-RLP-CBM formed much larger coacervates with a diameter near 1 μm (Figure 3b). The particle size obtained by the cryo-TEM was corresponding well with the DLS measurements. Without the addition of salts, there was no spherical coacervate particles formed in the CBM-RLP-CBM solutions, but there were some small protein agglomerates, which may have been the nucleation sites for the particles resulting from coacervation (Figure 3c). In the majority of protein aggregation events, the aggregation is initiated by formation of a nucleus, which could be a dimer or multimer.[27] The exon I-encoding polypeptide has been reported to self-aggregate into organized fibrillar structures on the basis of the backbone hydration and hydrogen bonding.[28] The small aggregates observed in the cryo-TEM images (Figure 3c) are likely the self-assemblies of CBM-RLP-CBM, which could grow to coacervate particles when salt was added.

A Cryo-TEM tilt series was collected from a single CBM-RLP-CBM coacervate and using electron tomographic reconstruction, the 3D structure of the particle was obtained. The relatively large size of the particles (> 1 μm) were found to be not suitable for Cryo-TEM tomography as they tended to flatten upon vitrification (see Electronic Supplementary Information Figure S3). This was expected as the ice thickness in vitrification for cryo-TEM is generally below 150 nm, whereas the coacervates were nearly 1 μm in diameter.[29] The flattening of the coacervate during the

vitrification also indicated that the CBM-RLP-CBM coacervate particles are dynamic and consist of extremely resilient liquid-like material.

In order to overcome the artefact of flattening during the cryo-TEM sample preparation, the coacervates were fixed on the TEM grid via sequential solvent exchange method.[30] Figure 4a-c presents the snapshots from tilt series suggesting nearly spherical shape of the coacervates (see video S1). 3D reconstruction of the aligned tilt series of the CBM-RLP-CBM coacervate is shown in Figure 4d further supporting the spherical shape. Interestingly, the internal structure of the coacervates using the cross section of the tomogram displayed ”onion-like” structures as shown in Figure 4e (see Electronic Supplementary Information, video S2). The similar onion-like structure was also observed in partially dehydrated cryo-TEM sample (see Figure S3). Therefore, we suspected that the “onion-like” structure might be induced by dehydration. The presence of artefacts due to missing wedge as well as due to drying cannot be ruled out.

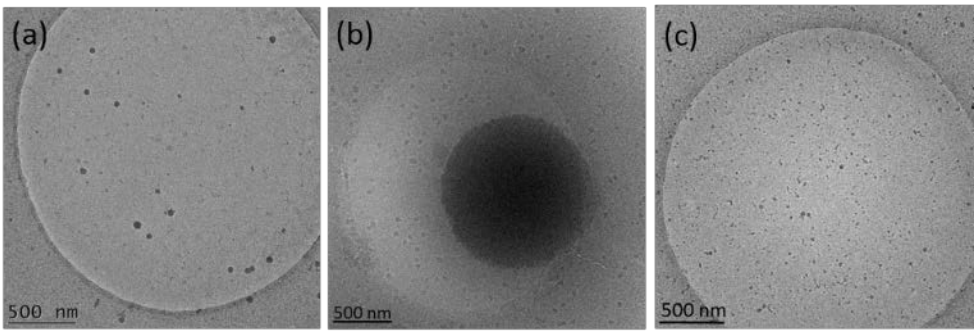

Figure 3. Cryo-TEM images of CBM-RLP-CBM coacervate formed at pH 4.5 sodium phosphate buffer (a) and pH 7.14 (b) with 5 g L^{-1} protein concentration. (c) 5 g L^{-1} CBM-RLP-CBM solution. The size of the coacervate increased at higher pH due to the extension of RLP molecule.

In Figure 4f, the SEM image of the CBM-RLP-CBM coacervate shows that its surface was not smooth, and it appeared to be composed of small particles. The *z*-stacking of the CBM-RLP-CBM coacervate by confocal microscopy showed that the fluorescence was evenly distributed within the

coacervates, which confirmed that their structure was quite homogeneous and not hollow (inset in Figure 4f).

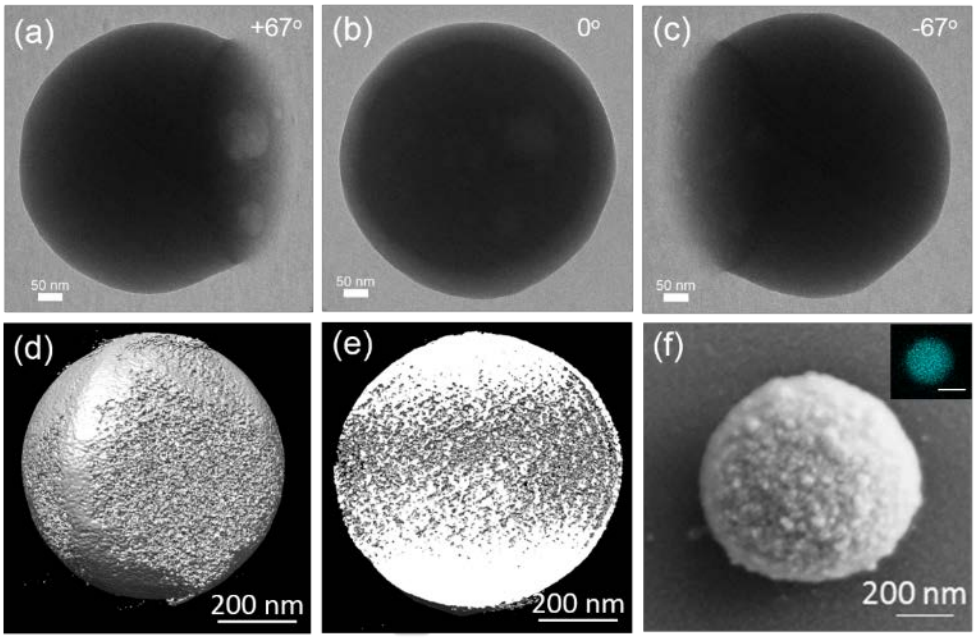

Figure 4. Structure characterization of CBM-RLP-CBM coacervate. (a) TEM micrographs at tilt angles of +67°; b) 0° and c) -67°; d) 3D reconstruction of CBM-RLP-CBM coacervate formed at pH 7.14 and the cross sectional view (e). (f) The SEM image of the coacervate dried by solvent exchanging. The inset in (f) is the confocal microscopy image. The scale bar is 1 μm.

The CBM-RLP-CBM coacervates typically occurred as individual particles, whereas the dCBM-RLP-HFBI coacervates were more likely to form clusters. The difference in the behavior of the coacervates was readily observed by imaging with optical microscope (videos S3 and S4 in the ESI). The dCBM-RLP-HFBI coacervates appeared to stick to each other and to form growing clusters, but the particles did not coalesce. It is known that in aqueous solutions, the hydrophobin HFBI has the tendency to form multimers due to the interactions between the hydrophobic patches in the proteins' structure.[31] Thus, the formation of the cluster of the dCBM-RLP-HFBI coacervates could possibly be explained by the hydrophobic interactions between the hydrophobins. This observation relates to our earlier study of the dCBM-RLP-HFBI molecule where

the forces related to the adhesion of the hydrophobin motif was studied by single molecule force spectroscopy.[17] At elevated pH, the strength of the hydrophobic interaction of the molecules was significantly higher compared to the forces measured at the IEP.[17] The reason for the large hydrophobic interaction of the dCBM-RLP-HFBI molecules was likely a consequence of the bundling of the extended resilin domains, which led to the formation of a larger hydrophobic patch as several hydrophobins were brought closely together. Thus, the coacervate cluster formation could be due to hydrophobic patches formed on the coacervate surface.

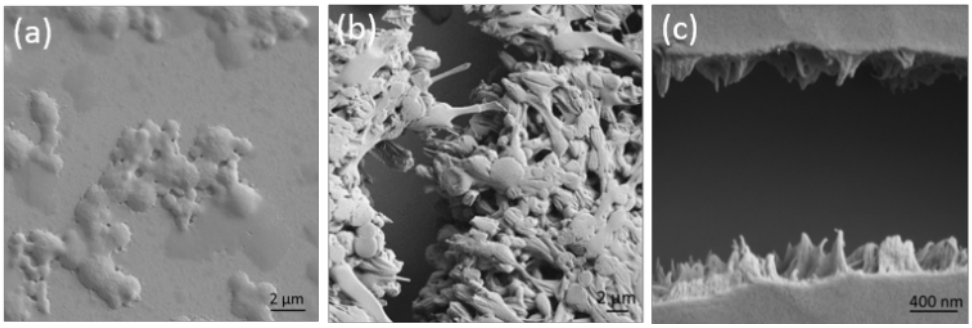

Figure 5. (a) SEM image of cross linked dCBM-RLP-HFBI coacervate dried at room temperature. The cross-linked coacervates were washed with water by centrifugation. (b) and (c) SEM image of dCBM-RLP-HFBI coacervate dried on silicon wafer at room temperature and heated at 70°C respectively. The coacervate was formed with 5 g L^{-1} protein and 500 mM phosphate buffer at pH 7.14.

The confocal microscopy image of the dCBM-RLP-HFBI coacervate taken under liquid environment showed that the cluster was composed of individual coacervates having spherical shape (Figure 2d). The morphology of the coacervate could be fixed by chemical cross-linking as shown in Figure 5a that represents a dried coacervate sample. When the non-cross-linked dCBM-RLP-HFBI coacervate sample was dried at room temperature, the particles were partly fused together and stretched into elongated shapes (Figure 5b). However, when the sample was dried at 70°C, the coacervate formed a smooth continuous film where fibrils were pulled out from the fractured surfaces (Figure 5c). The resilin exon I has shown to go through melting-like endothermic process at 50 °C, which appears to also happen for the coacervate leading to fusion of the

particles.[28] The fibril-like morphology was characteristic also for the fractured surfaces of the molten coacervate material. The cross-linked dCBM-RLP-HFBI coacervates, could resist the tension caused by drying and were able to keep their spherical shape as shown in Figure 5a.

Adhesion of the coacervates

We fused adhesive domains, CBM and HFBI to functionalize the resilin-like-peptides and consequently their coacervates. In previous work, it has been shown that CBMs and HFBI have specific affinities to cellulose and graphene surfaces, respectively.[32] Therefore, we investigated the adherence of dCBM-RLP-HFBI and CBM-RLP-CBM coacervates on graphene and cellulose surfaces by dip-coating the surfaces with coacervate suspension and assessing by SEM whether the particles adhered to the surface or not. The results of the adhesion test for all the three RLP variants are summarised in Figure 6 showing cellulose surfaces (a, d, g), graphene surfaces (b, e, h) and glass surfaces (c, f, i) after immersion to a smaple containing the coacervates. Glass was chosen as the control surface due to its hydrophilic nature and low surface charge that should not attract unspecific binding of the protein domains.

As shown in Figure 6a and b, the dCBM-RLP-HFBI coacervate adhered to both the graphene and cellulose surface forming a non-continuous layer on the surface. The CBM-RLP-CBM coacervate, however, could only adhere to the cellulose surface and not much on the graphene (Figures 6d and e). As in the liquid state, the CBM-RLP-CBM coacervates appeared separate micro-sized particles also when adsorbed on the surface. The RLP coacervate without any terminal domains adhered only on the graphene surface. None of the proteins significantly adhered to the glass surface.

The adhesion test showed that the functionality of the RLP fusion proteins was transferred to the microscopic coacervate particles. The hydrophobin containing coacervates showed the highest tendency towards adhesive behaviour. Adhesion of the RLP on the graphene surface indicated

that the hydrophobic amino acids in the non-structured RLP may become exposed and drive attachment on a hydrophobic surface. When flanked with the CBMs, the RLP molecule however, seemed resistant for the attraction of the hydrophobic surface.

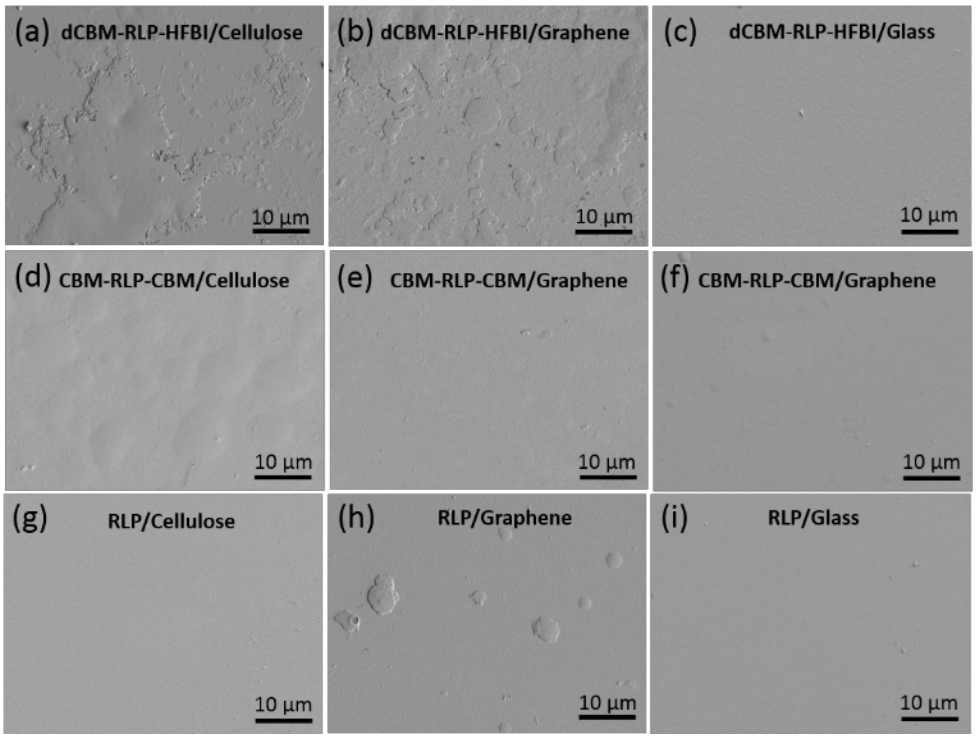

Figure 6. SEM images of RLP fusion proteins bind to different surfaces (a) dCBM-RLP-HFBI coacervates adsorbed on regenerated cellulose surface, (b) graphene surface and (c) glass surface. (d) CBM-RLP-CBM coacervates on regenerated cellulose surface, (e) graphene surface and (f) glass. (g) RLP coacervates adsorbed on regenerated cellulose surface, (h) graphene surface and (i) glass. The coacervates were formed with 5 g L^{-1} protein and 500 mM phosphate buffer at pH 7.14. The silicon wafer with different coatings or glass were dipping into the coacervate sample, rinsing with water gently and then dried at ambient conditions.

Conclusions

In conclusion, we have compared the pH induced coacervation of three different protein constructs: RLP, CBM-RLP-CBM and dCBM-RLP-HFBI. The RLP and CBM-RLP-CBM formed individual

coacervates, while the dCBM-RLP-HFBI formed coacervate clusters due to the hydrophobic interactions of HFBI. We also demonstrated that coacervate with specific affinity to different surfaces could be designed by fusion of functional terminal domains. The electron tomography study of individual coacervate revealed the porous structure of the coacervate particles. Besides, the size of the individual resilin coacervate could be modulated by pH, temperature and salt concentration. This study gives us a better understanding of the coacervation process of engineered resilin-like polypeptides and give the first sight of designing functional resilin coacervates, which have a large potential for applications in composite materials.

Acknowledgements

Riitta Suihkonen is thanked for the technical assistance in the protein purification. We thank Teemu Myllymäki for the help with ATR-FTIR. The authors acknowledge the Academy of Finland Center of Excellence Program, especially the Center of Excellence in Molecular Engineering of Biosynthetic Hybrid Materials (HYBER). This work made use of the facilities at the Aalto University Nanomicroscopy Center (Aalto-NMC) premises.

References

[1] P. Strzyz, Protein droplets in the spotlight, Nat. Rev. Mol. Cell Biol. 16 (2015) 639. doi:10.1038/nrm4070.

[2] A.W. Clarke, E.C. Arnspang, S.M. Mithieux, E. Korkmaz, F. Braet, A.S. Weiss, Tropoelastin massively associates during coacervation to form quantized protein spheres, Biochemistry. 45 (2006) 9989–9996. doi:10.1021/bi0610092.

[3] B. Vrhovski, S. Jensen, A.S. Weiss, Coacervation characteristics of recombinant human tropoelastin., Eur. J. Biochem. 250 (1997) 92–98. doi:10.1111/j.1432-1033.1997.00092.x.

[4] Y. Tu, S.G. Wise, A.S. Weiss, Stages in tropoelastin coalescence during synthetic elastin hydrogel formation, Micron. 41 (2010) 268–272. doi:10.1016/j.micron.2009.11.003.

[5] G.C. Yeo, F.W. Keeley, A.S. Weiss, Coacervation of tropoelastin, Adv. Colloid Interface Sci. 167 (2011) 94–103. doi:10.1016/j.cis.2010.10.003.

[6] H. Jiang, S. Wang, Y. Huang, X. He, H. Cui, X. Zhu, Y. Zheng, Phase Transition of Spindle-Associated Protein Regulate Spindle Apparatus Assembly, Cell. 163 (2015) 108–122. doi:10.1016/j.cell.2015.08.010.

[7] Y. Tan, S. Hoon, P.A. Guerette, W. Wei, A. Ghadban, C. Hao, A. Miserez, J.H. Waite, Infiltration of chitin by protein coacervates defines the squid beak mechanical gradient, Nat. Chem. Biol. 11 (2015) 488–495. doi:10.1038/nchembio.1833.

[8] W. Wei, Y. Tan, N.R. Martinez Rodriguez, J. Yu, J.N. Israelachvili, J.H. Waite, A mussel-derived one component adhesive coacervate, Acta Biomater. 10 (2014) 1663–1670. doi:10.1016/j.actbio.2013.09.007.

[9] C.M. Elvin, A.G. Carr, M.G. Huson, J.M. Maxwell, R.D. Pearson, T. Vuocolo, N.E. Liyou, D.C.C. Wong, D.J. Merritt, N.E. Dixon, Synthesis and properties of crosslinked recombinant pro-resilin., Nature. 437 (2005) 999–1002. doi:10.1038/nature04085.

[10] R. Balu, R. Knott, N.P. Cowieson, C.M. Elvin, A.J. Hill, N.R. Choudhury, N.K. Dutta, Structural ensembles reveal intrinsic disorder for the multi-stimuli responsive bio-mimetic protein Rec1-resilin, Sci. Rep. 5 (2015) 10896–10908. doi:10.1038/srep10896.

[11] R. Balu, N.K. Dutta, N.R. Choudhury, C.M. Elvin, R.E. Lyons, R. Knott, A.J. Hill, An16-resilin: An advanced multi-stimuli-responsive resilin-mimetic protein polymer, Acta Biomater. 10 (2014) 4768–4777. doi:10.1016/j.actbio.2014.07.030.

[12] L. Li, T. Luo, K.L. Kiick, Temperature-Triggered Phase Separation of a Hydrophilic Resilin-Like Polypeptide., Macromol. Rapid Commun. 36 (2015) 90–95. doi:10.1002/marc.201400521.

[13] H. Palonen, M. Tenkanen, M. Linder, Dynamic interaction of Trichoderma reesei cellobiohydrolases Cel6A and Cel7A and cellulose at equilibrium and during hydrolysis, Appl. Environ. Microbiol. 65 (1999) 5229–5233.

[14] A. Várnai, M.R. Mäkelä, D.T. Djajadi, J. Rahikainen, A. Hatakka, L. Viikari, Carbohydrate-Binding Modules of Fungal Cellulases. Occurrence in Nature, Function, and Relevance in Industrial Biomass Conversion, Adv. Appl. Microbiol. 88 (2014) 103–165. doi:10.1016/B978-0-12-800260-5.00004-8.

[15] M.B. Linder, G.R. Szilvay, T. Nakari-Setälä, M.E. Penttilä, Hydrophobins : the protein-amphiphiles of filamentous fungi, FEMS Microbiol. Rev. 29 (2005) 877–896. doi:10.1016/j.femsre.2005.01.004.

[16] W. Fang, A. Paananen, M. Vitikainen, S. Koskela, A. Westerholm-Parvinen, J.J. Joensuu, C.P. Landowski, M. Penttilä, M.B. Linder, P. Laaksonen, Elastic and pH-Responsive Hybrid Interfaces Created with Engineered Resilin and Nanocellulose, Biomacromolecules. 18 (2017) 1866–1873. doi:10.1021/acs.biomac.7b00294.

[17] A. Griffo, H. Hähl, S. Grandthyll, A. Paananen, A. Westerholm-Parvinen, R. Szilvay, G., C. Landowski, M.E. Penttilä, K. Jacobs, P. Laaksonen, Single molecule force spectroscopy study on modular resilin fusion protein, ACS Omega. (2017) Accepted.

[18] D. Mastronarde, SerialEM A Program for Automated Tilt Series Acquisition on Tecnai Microscopes Using Prediction of Specimen Position, Microsc. Microanal. 9 (2003) 1182–1183. doi:10.1017/S1431927603445911.

[19] J.R. Kremer, D.N. Mastronarde, J.R. McIntosh, Computer visualization of three-dimensional image data using IMOD., J. Struct. Biol. 116 (1996) 71–76. doi:10.1006/jsbi.1996.0013.

[20] P. Engelhardt, Electron Tomography of Chromosome Structure, Encycl. Anal. Chem. (2000) 4948–4984. doi:10.1002/9780470027318.a1405.

[21] J. Riikonen, W. Kim, C. Li, O. Svensk, S. Arpiainen, M. Kainlauri, H. Lipsanen, Photo-thermal chemical vapor deposition of graphene on copper, Carbon N. Y. 62 (2013) 43–50. doi:10.1016/j.carbon.2013.05.050.

[22] T. Mohan, R. Kargl, A. Doliška, A. Vesel, S. Köstler, V. Ribitsch, K. Stana-Kleinschek, Wettability and surface composition of partly and fully regenerated cellulose thin films from trimethylsilyl cellulose, J. Colloid Interface Sci. 358 (2011) 604–610. doi:10.1016/j.jcis.2011.03.022.

[23] A.M. Tamburro, S. Panariello, V. Santopietro, A. Bracalello, B. Bochicchio, A. Pepe, Molecular and supramolecular structural studies on significant repetitive sequences of resilin, ChemBioChem. 11 (2010) 83–93.

[24] S. Mayavan, N.K. Dutta, N.R. Choudhury, M. Kim, C.M. Elvin, A.J. Hill, Self-organization, interfacial interaction and photophysical properties of gold nanoparticle complexes derived from resilin-mimetic fluorescent protein rec1-resilin, Biomaterials. 32 (2011) 2786–2796.

[25] D.W. Urry, B. Starcher, S.M. Partridge, Coacervation of solubilized elastin effects a notable conformational change., Nature. 222 (1969) 795–796. doi:10.1038/222795a0.

[26] M.Y. Truong, N.K. Dutta, N.R. Choudhury, M. Kim, C.M. Elvin, A.J. Hill, B. Thierry, K. Vasilev, A pH-responsive interface derived from resilin-mimetic protein Rec1-resilin, Biomaterials. 31 (2010) 4434–4446.

[27] W. Wang, S. Nema, D. Teagarden, Protein aggregation-Pathways and influencing factors, Int. J. Pharm. 390 (2010) 89–99. doi:10.1016/j.ijpharm.2010.02.025.

[28] G. Qin, X. Hu, P. Cebe, D.L. Kaplan, Mechanism of resilin elasticity., Nat. Commun. 3 (2012) 1003–

1011.
http://www.pubmedcentral.nih.gov/articlerender.fcgi?artid=3527747&tool=pmcentrez&rendertype=abstract.

[29] H.-J. Cho, J.-K. Hyun, J.-G. Kim, H.S. Jeong, H.N. Park, D.-J. You, H.S. Jung, Measurement of ice thickness on vitreous ice embedded cryo-EM grids: investigation of optimizing condition for visualizing macromolecules, J. Anal. Sci. Technol. 4 (2013) 7. doi:10.1186/2093-3371-4-7.

[30] K. Bertula, Nonappa., T.T.T. Myllymäki, H. Yang, X.X. Zhu, O. Ikkala, Hierarchical Self-Assembly from Nanometric Micelles to Colloidal Spherical Superstructures, Prep. (2017).

[31] G.R. Szilvay, T. Nakari-Setälä, M.B. Linder, Behavior of Trichoderma reesei hydrophobins in solution: Interactions, dynamics, and multimer formation, Biochemistry. 45 (2006) 8590–8598.

[32] P. Laaksonen, A. Walther, J.-M. Malho, M. Kainlauri, O. Ikkala, M.B. Linder, Hybrid Nanocomposites from Graphene, Nanocellulose and Genetically Engineered Proteins, Angew. Chem. Int. Ed. Linder Biomacromolecules Phys. Chem. Chem. Phys. Sci. 50 (2011) 8688–8691.